

An Improved Fractional-Order Active Disturbance Rejection Control: Performance Analysis and Experiment Verification

Bolin Li, Lijun Zhu,

Abstract—This paper presents an improved active disturbance rejection control scheme (IFO-ADRC) with an improved fractional-order extended state observer (IFO-ESO). The structural information of the system is utilized in IFO-ESO rather than buried as in the typical fractional-order extended state observer (FO-ESO) and help significantly improve the performance of IFO-ESO and closed-loop system. Compared with the integer-order active disturbance rejection controller (IO-ADRC), the auxiliary tracking controller of IFO-ADRC has a simpler form and fewer parameters need to be tuned. Frequency-domain analysis shows that IFO-ESO has better performance over the larger frequency band than FO-ESO, and time-domain simulation shows that IFO-ADRC has better transient performance and is more robust against the parameter variations than traditional fractional-order active disturbance rejection controller (FO-ADRC) and IO-ADRC. The IFO-ADRC is applied to permanent magnet synchronous motor (PMSM) servo control system and demonstrates its capability in the real-world application.

Index Terms—ctive disturbance rejection control, fractional-order active disturbance rejection control, fractional-order extended state observer, robustness.ctive disturbance rejection control, fractional-order active disturbance rejection control, fractional-order extended state observer, robustness.A

I. INTRODUCTION

FRACTIONAL calculus has been applied to different fields in recent years [1], [2], [3], [4]. With a deep understanding of the system, there is a growing need for fractional-order control and modelling [5], [6]. Some real-world phenomena demonstrate fractional-order characteristics [7], [8]. Permanent magnet synchronous motor [8], gas-turbine [9], and heating-furnace [10] can be identified as fractional-order models. On the other hand, the fractional-order controller has the potential to achieve better and more robust control performance than the integer-order controller [11]. Many fractional-order controllers have been proposed, including fractional-order sliding mode controller [12], [13], fractional-order intelligent PID controller [14], fractional-order PID controller [15], and so on.

The active disturbance rejection control (ADRC) was proposed in [16] as an alternative paradigm for control system design. The core idea of ADRC is to improve the robustness of the system using extended state observer (ESO). ESO, an

important part ADRC, can estimate the total disturbances, including internal disturbance caused by system uncertainties and external disturbance. Gao [17] proposed the linear ADRC to broaden the application range of ADRC by linearizing ESO (IO-ESO) and feedback control law. Applying IO-ESO, a m -order integer-order system can be approximately converted into m unit gain integer-order integrators in series. According to the design idea of the linear IO-ADRC, a linear feedback control law of m parameters need to be designed to realize the stable closed-loop system. Furthermore, Gao [18] proposed an ADRC structure involving the fractional-order tracking differentiator, the fractional-order PID controller and the fractional-order extended state observer for nonlinear fractional-order systems. The stability region of the fractional-order system can be larger than that of the integer-order system in the complex plane [19]. FO-ADRC can provide a possibility to realize closed-loop stability with a simpler controller. In [1], Chen et al. applied FO-ESO to approximately convert a typical second-order system into a cascaded fractional-order integrator and the stable closed-loop system can be realized using merely a simple proportional controller. For a fractional-order system, it is natural to use a fractional-order controller to achieve closed-loop stability [20], [21]. A FO-ADRC based on FO-ESO was proposed by Li [22] to approximately convert the fractional-order system to a cascaded fractional-order integrator. The IO-ADRC was proved by Li [23] to estimate the disturbances in fractional-order systems, which considers the fractional-order dynamics as a common disturbance.

An integer-order system can be approximately converted to a fractional-order system (a cascaded fractional-order integrator) by using FO-ESO and then an auxiliary tracking controller is designed to meet the actual needs [1]. However, the satisfactory approximation can only be made in the low-frequency band, making it difficult to ensure the system's robustness when the control system bandwidth is large. This paper is along the research line of proposing a new type of fractional-order ESO structure and then fractional-order ADRC. The main contributions of the paper can be summarized as follows. First, the new type of ESO, called IFO-ESO, will utilize structural information in the total disturbance given in FO-ESO. IFO-ESO will be used to compensate for the system uncertainties and external disturbance. The compensated system is approximately converted into a fractional-order integrator. It will be shown that the approximation performance is improved by IFO-ESO over FO-ESO, making the system more robust to system uncertainties and external

Bolin Li is with Key Laboratory of Imaging Processing and Intelligence Control, School of Artificial Intelligence and Automation, Huazhong University of Science and Technology, Wuhan 430074, China.

Lijun Zhu is with Key Laboratory of Imaging Processing and Intelligence Control, School of Artificial Intelligence and Automation, Huazhong University of Science and Technology, Wuhan 430074, China.

disturbances. The theoretical analysis is verified by the control experiment on the PMSM servo speed control system. Second, compared with IO-ADRC, the auxiliary tracking controller of IFO-ADRC has a simpler form and fewer parameters need to be tuned. Thirdly, the stability criteria of the IFO-ESO and the IFO-ADRC closed-loop system are given when the disturbance is assumed to be bounded. Unlike the stability analysis of the ESO and the closed-loop system in [1] and [22], the stability criteria of the high-order ESO and high-order ADRC closed-loop system in this paper are given.

This paper is organized as follows. The structures of IFO-ESO and IFO-ADRC are proposed in Section II. The BIBO stability criteria of the IFO-ESO and the closed-loop system are given in Section III. The performance analysis of the IFO-ESO in the frequency-domain is shown in Section IV. Section V presents the time-domain simulation results, followed by the experimental results on PMSM servo system in VI. The paper is concluded in Section VII.

Notations. I_n is an $n \times n$ identity matrix and $0_{n \times m}$ is a zero vector matrix with size specified by the subscript.

II. AN IMPROVED STRUCTURE OF ACTIVE DISTURBANCE REJECTION CONTROLS

In this paper, we consider an integer-order linear system as follows:

$$G(s) = \frac{Y(s)}{U(s)} = \frac{b}{s^m + \sum_{i=1}^{m-1} a_i s^i + a_0} \quad (1)$$

where s is Laplace operator, a_i , a_0 and b are real numbers, m and i are positive integers with m representing the maximum order of the system. The differential equation form of system (1) with the external disturbance, denoted by d , is

$$y^{(m)} = - \sum_{i=1}^{m-1} a_i y^{(i)} - a_0 y + bu + d \quad (2)$$

Caputo derivative is adopted as the fractional-order derivative method in this paper and described as follows,

$$f^{(\gamma)}(t) = {}_0^C D_t^\gamma f(t) = \frac{1}{\Gamma(m_0 - \gamma)} \int_0^t \frac{f^{(m_0)}(\tau)}{(t - \tau)^{\gamma - m_0 + 1}} d\tau \quad (3)$$

where m_0 is an integer satisfying $m_0 - 1 < \gamma < m_0$ and γ is a real number, $\Gamma(\bullet)$ is Euler's gammafunction. From the adopted definition, one can see that ${}_0^C D_t^\gamma f(t)^{(\vartheta)} = {}_0^C D_t^{\gamma + \vartheta} f(t)$ where ϑ is a positive number [24].

Let $\bar{\gamma}$ be a fractional number satisfying $m - 1 < \bar{\gamma} < m$, n be a positive integer number satisfying $\bar{\gamma} < n < \frac{\bar{\gamma}}{m - \bar{\gamma}}$, and $\gamma = \frac{\bar{\gamma}}{n}$ be a fractional number. As a result, $n\gamma < m < (n+1)\gamma$. Define the quantity $q(y^{(n\gamma)}, y^{(m)}, t) = y^{(n\gamma)} - y^{(m)}$. Equation

(2) can be rewritten as follows,

$$\begin{aligned} y^{(n\gamma)} &= y^{(n\gamma)} - y^{(m)} - \sum_{i=1}^{m-1} a_i y^{(i)} - a_0 y + bu + d \\ &= y^{(n\gamma)} - y^{(m)} - \sum_{i=1}^{m-1} a_i y^{(i)} - a_0 y + (b - b_0)u \\ &\quad + b_0 u + d \\ &= q(y^{(n\gamma)}, y^{(m)}, t) + f_{ifo}(y^{(1)}, y^{(2)}, \dots, y^{(m-1)}, y, u, t) \\ &\quad + b_0 u \end{aligned} \quad (4)$$

Note that $f_{ifo} = - \sum_{i=1}^{m-1} a_i y^{(i)} - a_0 y + (b - b_0)u + d$ can be regarded as the total disturbance where the term $-\sum_{i=1}^{m-1} a_i y^{(i)} - a_0 y + (b - b_0)u$ is the internal disturbance due to uncertain parameters and d is the external disturbance. The aim of this paper is to design u such that the system output tracks a sufficiently smooth reference trajectory r and the ultimate tracking error stays in the neighborhood of the origin, i.e., $\lim_{t \rightarrow \infty} \|y(t) - r(t)\| < \epsilon$, when the reference signal and its derivatives, i.e., $r, \dot{r}, \ddot{r}, \dots, r^{(m-1)}, r^{(n\gamma - m + 1)}$, are bounded.

As inspired by FO-ADRC in [1], we propose the tracking controller as follows

$$u = \frac{u_0 - \hat{q} - \hat{f}_{ifo}}{b_0} \quad (5)$$

where \hat{q} and \hat{f}_{ifo} are estimators for signals q and f_{ifo} , respectively, and u_0 is the auxiliary tracking controller to be specified later. If signals q and f_{ifo} are approximately estimated by \hat{q} and \hat{f}_{ifo} , the closed-loop system composed of (4) and (5) can be approximately converted into a fractional-order integrator as follows

$$y^{(n\gamma)} = u_0 + (f_{ifo} - \hat{f}_{ifo}) + (q - \hat{q}) \approx u_0. \quad (6)$$

As will be explained in Remark 2.2, a big advantage of IFO-ADRC and FO-ADRC is that a simpler auxiliary controller can be designed and easily tuned.

Remark 2.1: For FO-ADRC in [1], equation (2) is written as

$$\begin{aligned} y^{(n\gamma)} &= f_{fo}(y^{(1)}, y^{(2)}, \dots, y^{(m-1)}, y^{(n\gamma)}, y^{(m)}, y, u, t) \\ &\quad + b_0 u \end{aligned} \quad (7)$$

where the term $f_{fo} = y^{(n\gamma)} - y^{(m)} - \sum_{i=1}^{m-1} a_i y^{(i)} - a_0 y + (b - b_0)u$. In comparison to FO-ADRC, IFO-ADRC will separate the structurally certain term q from f_{fo} . It is explicitly included in (4) and estimated in a new type of ESO introduced later. As will be demonstrated in Section IV and V, the structural certainty of the term q can help significantly improve the performance of ESO and the closed-loop system. ■

Let $x_1 = y, x_2 = y^{(\gamma)}, \dots, x_n = y^{((n-1)\gamma)}, x_{n+1} = f_{ifo}, h_{ifo} = f_{ifo}^{(\gamma)}(y^{(1)}, y^{(2)}, \dots, y^{(m-1)}, y, u, t)$ where

x_1, x_2, \dots, x_n represent system states and x_{n+1} is an extended state, the state-space representation of (4) is given as follows:

$$\begin{cases} \dot{x}^{(\gamma)} = Ax + Bu + Eh_{ifo} + Fq \\ y = Cx \end{cases} \quad (8)$$

where

$$\begin{aligned} x &= [x_1, x_2, \dots, x_n, x_{n+1}]^T, A = \begin{bmatrix} 0_{n \times 1} & I_n \\ 0 & 0_{1 \times n} \end{bmatrix} \\ B &= [0, 0, \dots, b_0, 0]^T, C = [1, 0, \dots, 0, 0], \\ E &= [0 \ \dots \ 0 \ 1]^T, F = [0 \ \dots \ 0 \ 1 \ 0]^T. \end{aligned} \quad (9)$$

Then, IFO-ESO is designed to estimate $x_1, x_2 \dots x_n, x_{n+1}$ as follows:

$$\begin{aligned} \dot{z}^{(\gamma)} &= Az + Bu + F\hat{q} + L(y - \hat{y}) \\ \hat{y} &= Cz \end{aligned} \quad (10)$$

where

$$\begin{aligned} z &= [z_1, z_2, \dots, z_n, z_{n+1}]^T \\ L &= [\beta_1, \beta_2, \dots, \beta_n, \beta_{n+1}]^T \\ \hat{q} &= (z_n^{(\gamma)} - z_n^{(m-n\gamma+\gamma)}) \end{aligned} \quad (11)$$

Note that L are extended state observer gains. $z_1, z_2, \dots, z_n, z_{n+1}$ are the estimation of the state $x_1, x_2, \dots, x_n, x_{n+1}$, respectively and b_0 is the nominal value of b . Let \hat{f}_{ifo} in (5) be $\hat{f}_{ifo} = z_{n+1}$.

With IFO-ESO, the tracking task can be fulfilled with the auxiliary tracking controller u_0 in (5), which is designed as follows,

$$\begin{aligned} u_0 &= k_p(r - z_1) + k_{d_1}(\dot{r} - \dot{z}_1) + \dots \\ &+ k_{d_{m-2}}(r^{(m-2)} - z_1^{(m-2)}) + r^{(n\gamma)} \end{aligned} \quad (12)$$

where $k_p, k_{d_1}, \dots, k_{d_{m-2}}$ are the parameters of the feedback control law. The closed-loop system composed of (2), (5) and (12), is called IFO-ADRC system.

Remark 2.2: For IO-ADRC in [17], the (2) is written as

$$y^{(m)} = f_{io}(y^{(1)}, y^{(2)}, \dots, y^{(m-1)}, y, u, t) + b_0 u$$

where $f_{io} = -\sum_{i=1}^{m-1} a_i y^{(i)} - a_0 y + (b - b_0)u$. Any part of controller similar to (5) where the auxiliary tracking controller u_0 is designed as

$$\begin{aligned} u_0 &= k_p(r - z_1) + k_{d_1}(\dot{r} - \dot{z}_1) + \dots \\ &+ k_{d_{m-1}}(r^{(m-1)} - z_1^{(m-1)}) + r^{(m)}, \end{aligned} \quad (13)$$

Note that the number of parameters for the auxiliary tracking controller of IFO-ADRC is less than that of IO-ADRC. In other words, we can achieve the trajectory tracking for an integer-order plant with a simpler auxiliary controller u_0 process, which simplifies the parameter tuning. As will be demonstrated in Section V, a P auxiliary tracking controller can be adopted to achieve the trajectory tracking of a second-order integer-order plant, and a PD auxiliary tracking controller can be adopted for a third-order integer-order plant. Section V will show the system transient performance of IFO-ADRC is better than that of IO-ADRC. ■

III. STABILITY ANALYSIS OF IFO-ADRC

In this section, the stability criteria for the ESO and the IFO-ADRC system are provided. Let the observer error be

$$e_i = x_i - z_i, i = 1, \dots, n + 1. \quad (14)$$

From (8) and (10), the equation of the extended state observer error can be written as

$$\dot{e}^{(\gamma)} = Ae - Le_1 + F(e_n^{(\gamma)} - e_n^{(m-n\gamma+\gamma)}) \quad (15)$$

where $e = [e_1, e_2, \dots, e_n, e_{n+1}]^T$. The characteristic matrix of (15) is [25]:

$$\lambda(s) = \begin{bmatrix} s^\gamma + \beta_1 & -1 & 0 & \dots & 0 & 0 \\ \beta_2 & s^\gamma & -1 & \dots & 0 & 0 \\ \vdots & \vdots & \vdots & \vdots & \vdots & \vdots \\ \beta_n & 0 & 0 & \dots & s^\gamma & -1 \\ \beta_{n+1} & 0 & 0 & \dots & 0 & s^\gamma \end{bmatrix} \quad (16)$$

From (16), the characteristic polynomial of the system (15) can be obtained:

$$\lambda(s) = s^{\nu+\gamma}(s^{n\gamma} + \sum_{i=1}^{n-1} \beta_i s^{(n-i)\gamma}) + \beta_n s^\gamma + \beta_{n+1} \quad (17)$$

where $\nu = m - n\gamma$ and $0 < \nu < \gamma$. Then, Theorem 3.1 will present the bounded-input bounded-output (BIBO) stability of the error system (15), when h_{ifo} is bounded. If the boundedness of the external disturbance d rather than h_{ifo} is assumed, Theorem 3.2 will give the condition of BIBO stability of the closed-loop system in terms of roots of a polynomial. In this case, the tracking error converges into a neighborhood of the origin. A special case of Theorem 3.2 when $m = n = 2$ is elaborated in Proposition 3.1, showing that when the observer gain is selected sufficiently large, the system is BIBO. The proofs of both theorems and the proposition are given in the Appendix.

Theorem 3.1: Consider the error dynamics of IFO-ESO (15). Let $\omega_o > 0$ and $\beta_i = C_{n+1}^i \omega_o^i$ for $i = 1, 2, \dots, n + 1$. If h_{ifo} is bounded, then the IFO-ESO is BIBO stable, regarding h_{ifo} as the input and e_1 as the output. ■

Theorem 3.2: Consider the IFO-ADRC closed-loop system composed of (2), (5) and (12). Let p_1, p_2, q_1 , and q_3 positive prime such that $\nu = \frac{p_1}{q_1}$ and $\gamma = \frac{p_2}{q_2}$. Define a polynomial

$$\begin{aligned} P(w) &= (w^{p_2 q_1} \sum_{i=0}^{m-1} a_i w^{i q_1 q_2}) (k_p + \sum_{i=1}^{m-2} k_{d_i} w^{i q_1 q_2}) \\ &+ w^{n p_2 q_1} + \sum_{i=1}^n \beta_i w^{(n-i) p_2 q_1} + (w^{n p_2 q_1} + k_p \\ &+ \sum_{i=1}^{m-2} k_{d_i} w^{i q_1 q_2}) (w^{p_1 q_2 + p_2 q_1} (w^{n p_2 q_1} + \sum_{i=1}^{n-1} \beta_i w^{(n-i) p_2 q_1}) \\ &+ \beta_n w^{p_2 q_1} + \beta_{n+1}) \end{aligned} \quad (18)$$

If $b = b_0, k_p, k_{d_1}, \dots, k_{d_{m-2}}$ and $\beta_1, \dots, \beta_{n+1}$ are selected such that all the roots of (18) are located in $|\arg(w_i)| > \frac{\pi}{2q_1 q_2}$, then the IFO-ADRC closed-loop system is BIBO stable,

Moreover, the tracking error $r(t) - y(t)$ converges to a small neighborhood of the origin as $t \rightarrow \infty$. ■

Proposition 3.1: Consider the IFO-ADRC closed-loop system composed of (2), (5) and (12) with $m = n = 2$. Suppose the plant (2) is stable or marginally stable, i.e., $a_1 \geq 0$ and $a_0 \geq 0$. Let $\beta_i = C_{n+1}^i \omega_o^i$ for $i = 1, 2, 3$, $k_p > 0$. Then, there always exists a constant $\omega_o > 0$, such that the closed-loop system is BIBO stable. Moreover, the tracking error $r(t) - y(t)$ converges to a small neighborhood of the origin as $t \rightarrow \infty$. ■

IV. PERFORMANCE ANALYSIS OF IFO-ESO IN FREQUENCY-DOMAIN

In this section, we will compare the performance of the IFO-ESO proposed in Section II with the FO-ESO proposed in [1]. The FO-ESO is as follows

$$\begin{aligned} z^{(\gamma)} &= Az + Bu + L(y - \hat{y}) \\ \hat{y} &= Cz \end{aligned} \quad (19)$$

where z , A , B , C and L are given in (11). Similar to the analysis in Section II, the controller u utilizing the estimation of the FO-ESO in [1] is

$$u = \frac{u_0 - \hat{f}_{fo}}{b_0} \quad (20)$$

which is aimed to approximately convert the perturbed system into a pure cascaded integrator shown as follows

$$y^{(n\gamma)} = u_0 + (f_{fo} - \hat{f}_{fo}) \approx u_0. \quad (21)$$

Note that the role of the ESO in the framework of ADRC including IO-ESO, FO-ESO and IFO-ESO is to estimate the uncertain dynamics and external disturbances to improve the robustness of the system. If the IFO-ESO can perfectly estimate \hat{q} and \hat{f}_{ifo} or the FO-ESO can perfectly estimate \hat{f}_{fo} , the IFO-ADRC in (5) and the FO-ADRC in (20) can convert the original system into a cascaded fractional-order integrator $1/s^{n\gamma}$ (looking from u_0 to y). Therefore, we are motivated to use the model difference between $Y(s)/U_0(s)$ and $1/s^{n\gamma}$ to assess the performance of the two ESO. We adopt mean square error between $Y(s)/U_0(s)$ and $1/s^{n\gamma}$ in the frequency-domain to evaluate how difference the two models are. The mean square error (MSE) of two linear model is defined as

$$e_o(\omega) = |\Delta_o(\omega)|^2 \quad (22)$$

where

$$\Delta_o(\omega) = 1 - (j\omega)^{n\gamma} Y(j\omega)/U_0(j\omega) \quad (23)$$

The MSE (22) was used in [26] for the model identification where the problem is re-casted into an optimal problem of minimizing the model difference between the identified and ideal model in terms of the MSE. Therefore, the MSE can be used to evaluate model difference in the frequency-domain.

As in [1], for simplicity, we consider the second-order system as follow

$$G(s) = \frac{Y(s)}{U(s)} = \frac{b_0}{s(s + a_o)}, \quad (24)$$

where the external disturbance and system uncertainty are not considered. In this case, the FO-ESO in (19) is simplified with

$$\begin{aligned} z &= [z_1, z_2, z_3]^T, \quad A = \begin{bmatrix} 0_{3 \times 1} & I_3 \\ 0 & 0_{1 \times 3} \end{bmatrix} \\ B &= [0, b_0, 0]^T, \quad C = [1, 0, 0]. \end{aligned} \quad (25)$$

Similarly, the IFO-ESO is

$$\begin{aligned} z^{(r)} &= Az + Bu + E\hat{q} + L(y - \hat{y}), \\ \hat{q} &= (z_2^{(\gamma)} - z_2^{(2-\gamma)}), \\ \hat{y} &= Cz, \end{aligned} \quad (26)$$

where $E = [0, 1, 0]^T$.

Next, let us calculate $Y(s)/U_0(s)$ for FO-ADRC and IFO-ADRC. For the fair comparison, we choose the same group of the observer gains $\beta_1 = 3\omega_o$, $\beta_2 = 3\omega_o^2$, $\beta_3 = \omega_o^3$ for IFO-ESO and FO-ESO. For the IFO-ESO, all the parameters meet the conditions of Theorem 3.1, and thus the dynamics of the estimation error for IFO-ESO is asymptotically stable (because the disturbance and uncertainties do not exist). Conducting the Laplace transform on the both sides of (26) gives

$$\begin{aligned} Z_1(s) &= \frac{(3\omega_o s^2 + 3\omega_o^2 s^\gamma + \omega_o^3)Y(s)}{s^{2+\gamma} + 3s^2\omega_o + 3s^\gamma\omega_o^2 + \omega_o^3} \\ &\quad + \frac{b_0 s^\gamma U(s)}{s^{2+\gamma} + 3s^2\omega_o + 3s^\gamma\omega_o^2 + \omega_o^3} \\ Z_2(s) &= \frac{(3\omega_o^2 s^{2\gamma} + \omega_o^3 s^\gamma)Y(s)}{s^{2+\gamma} + 3s^2\omega_o + 3s^\gamma\omega_o^2 + \omega_o^3} \\ &\quad + \frac{b_0 (s^{2\gamma} + 3\omega_o s^\gamma)U(s)}{s^{2+\gamma} + 3s^2\omega_o + 3s^\gamma\omega_o^2 + \omega_o^3} \\ Z_3(s) &= \frac{\omega_o^3 s^2 Y(s)}{s^{2+\gamma} + 3s^2\omega_o + 3s^\gamma\omega_o^2 + \omega_o^3} \\ &\quad - \frac{b_0 \omega_o^3 U(s)}{s^{2+\gamma} + 3s^2\omega_o + 3s^\gamma\omega_o^2 + \omega_o^3} \\ Q(s) &= (s^\gamma - s^{2-\gamma})Z_2(s) \end{aligned} \quad (27)$$

where $Z_1(s)$, $Z_2(s)$, $Y(s)$, $U(s)$ and $Q(s)$ are the Laplace transforms of signals z_1 , z_2 , y , and u , and the quantity q , respectively. Conducting the Laplace transform on the both sides of (5) and substituting the result and (27) into (24) obtain

$$P_{ifo}(s) = \frac{Y(s)}{U_0(s)} = \frac{N_1}{D_1} \quad (28)$$

where

$$\begin{aligned} N_1 &= b(s^{2+\gamma} + 3s^2\omega_o + 3s^\gamma\omega_o^2 + \omega_o^3) \\ D_1 &= b\omega_o^2 s^\gamma (-3s^2 + 3s^{2\gamma} + s^\gamma\omega_o) \\ &\quad + a_o b_0 s^{1+\gamma} (s^{2\gamma} + 3s^\gamma\omega_o + 3\omega_o^2) \\ &\quad + b_0 s^{2+\gamma} (s^{2\gamma} + 3s^\gamma\omega_o + 3\omega_o^2) \end{aligned} \quad (29)$$

Similarly, the Laplace transform of the both side of FO-ESO

(19) gives

$$\begin{aligned}
Z_1(s) &= \frac{(3\omega_o s^{2\gamma} + 3\omega_o^2 s^\gamma + \omega_o^3)Y(s)}{s^{3\gamma} + 3s^{2\gamma}\omega_o + 3s^\gamma\omega_o^2 + \omega_o^3} \\
&\quad + \frac{b_0 s^\gamma U(s)}{s^{3\gamma} + 3s^{2\gamma}\omega_o + 3s^\gamma\omega_o^2 + \omega_o^3} \\
Z_2(s) &= \frac{(3\omega_o^2 s^{2\gamma} + \omega_o^3 s^\gamma)Y(s)}{s^{3\gamma} + 3s^{2\gamma}\omega_o + 3s^\gamma\omega_o^2 + \omega_o^3} \\
&\quad + \frac{b_0 (s^{2\gamma} + 3\omega_o s^\gamma)U(s)}{s^{3\gamma} + 3s^{2\gamma}\omega_o + 3s^\gamma\omega_o^2 + \omega_o^3} \\
Z_3(s) &= \frac{\omega_o^3 s^2 Y(s)}{s^{3\gamma} + 3s^{2\gamma}\omega_o + 3s^\gamma\omega_o^2 + \omega_o^3} \\
&\quad - \frac{b_0 \omega_o^3 U(s)}{s^{3\gamma} + 3s^{2\gamma}\omega_o + 3s^\gamma\omega_o^2 + \omega_o^3}
\end{aligned} \tag{30}$$

Conducting the Laplace transform on the both sides of (20) and substituting the result and (30) into (24) obtain

$$P_{fo}(s) = \frac{Y(s)}{U_0(s)} = \frac{N_2}{D_2} \tag{31}$$

where

$$\begin{cases} N_2 = b(s^\gamma + \omega_o)^3 \\ D_2 = bs(a_o + s)(s^\gamma + \omega_o)^3 \\ \quad + (bs^{2\gamma} - b_0 s^2 - a_o b_0 s)\omega_o^3 \end{cases} \tag{32}$$

The model difference between the fractional-order integrator ($1/s^{2\gamma}$) and P_o (P_{ifo} or P_{fo}) at ω can be expressed as:

$$\Delta_o = 1 - (j\omega)^{2\gamma} P_o(j\omega) \tag{33}$$

Then, the mean-square error between the fractional-order integrator and P_{ifo} can be expressed as follows:

$$\Delta_{ifo} = \frac{N_3}{D_3} \tag{34}$$

where

$$\begin{aligned} N_3 &= a_o j\omega((j\omega)^{2\gamma} + 3\omega_o(j\omega)^\gamma + 3\omega_o^2) \\ D_3 &= a_o j\omega((j\omega)^{2\gamma} + 3\omega_o(j\omega)^\gamma + 3\omega_o^2) + (j\omega)^\gamma((j\omega)^{2+\gamma} \\ &\quad + 3\omega_o(j\omega)^2 + 3\omega_o^2(j\omega)^\gamma + \omega_o^3) \end{aligned} \tag{35}$$

From (22) and (31), the mean-square error between the fractional-order integrator and P_{fo} can be expressed as follows:

$$\Delta_{fo} = \frac{N_4}{D_4} \tag{36}$$

where

$$\begin{aligned} N_4 &= \omega_o^3(j\omega)^\gamma - (j\omega)^\gamma((j\omega)^\gamma + \omega_o)^3 \\ &\quad + (a_o j\omega + (j\omega)^2)((j\omega)^{2\gamma} + 3\omega_o(j\omega)^\gamma + 3\omega_o^2) \\ D_4 &= \omega_o^3(j\omega)^\gamma + (a_o j\omega \\ &\quad + (j\omega)^2)((j\omega)^{2\gamma} + 3\omega_o(j\omega)^\gamma + 3\omega_o^2) \end{aligned} \tag{37}$$

Now, let us use the Bode diagram to study the performance of FO-ESO and IFO-ESO with observer gains $L = [3\omega_0, 3\omega_0^2, \omega_0^3]^T$. Moreover, the system parameters and the observer gain parameters are adapted from [1], i.e., $a_o = 26.08$, $b_0 = 383.635$, $\omega_o = 700$ and $\gamma = 0.75$. The Bode diagram of P_{ifo} in (28) and P_{fo} in (31) are illustrated in Fig. 1. It is clearly shown in Fig. 1 that the amplitude and the phase diagram of P_{ifo} are close to that of $1/s^{1.5}$ within a

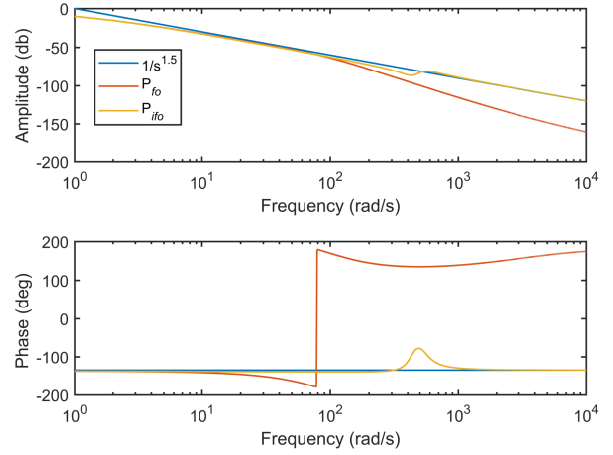


Fig. 1. Bode diagram of the model $Y(s)/U_o(s)$: P_{ifo} in (28) with IFO-ESO; P_{fo} in (31) with FO-ESO.

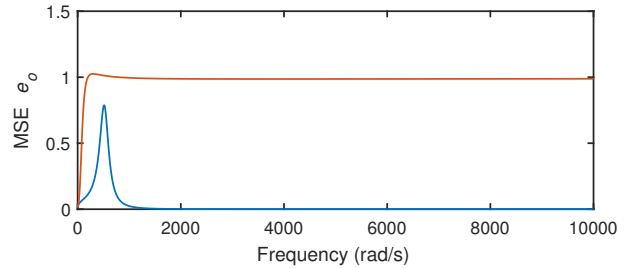


Fig. 2. The MSE curves when $a_o = 26.08$, $\gamma = 0.75$, and $\omega_o = 700$

larger frequency band than that of P_{fo} are. In particular, the approximation of P_{fo} to $1/s^{1.5}$ gets worse in high-frequency band. Fig. 2 shows the mean-square error e_{fo} and e_{ifo} with respect to frequency ω . The result coincides with Fig. 1 that P_{ifo} better approximates the integrator $1/s^{1.5}$ than P_{fo} does. In other words, the IFO-ESO has better performance in terms of disturbance estimation than the FO-ESO. Therefore, the closed-loop system resulting from the IFO-ESO is more robust than that from the FO-ESO.

Fig. 3 shows the curves of the mean-square error e_{fo} and e_{ifo} with different model parameter a_o when $\omega_o = 2000$ and $\gamma = 0.75$. Fig. 4 shows the curves of the mean-square error e_{fo} and e_{ifo} with different observer gains ω_o when $a_o = 10$ and $\gamma = 0.75$. Fig. 5 demonstrates the variation of the mean-square error with different order γ when $a_o = 10$ and $\omega_o = 2000$. As shown in Fig. 3, Fig. 4, and Fig. 5, the mean-square error e_{ifo} is less prone to the variation of system parameter a_o , controller parameters ω_o , and the order γ than the mean-square error e_{fo} is.

Remark 4.1: Note that if the performance of ESO is robust to the variation of the closed-loop system parameters a_o , ω_o , and γ , the auxiliary tracking controller design of u_0 based on the compensated system (6) or (21) can achieve better performance when these parameters vary. In other words, the IFO-ADRC closed-loop system is more robust with respect to the variations of the plant $G(s)$ parameters and ESO

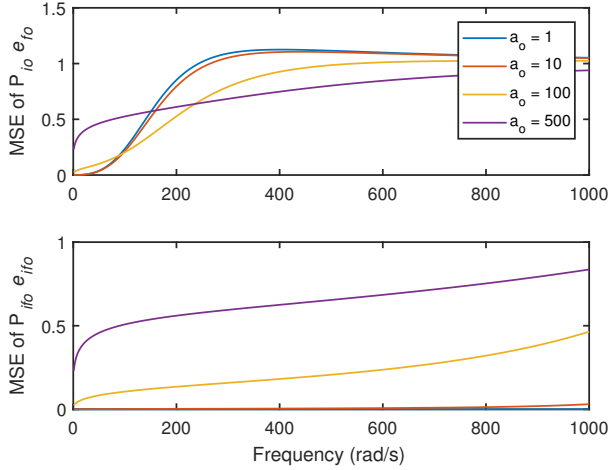


Fig. 3. The MSE curves with different a_o when $\omega_o = 2000$ and $\gamma = 0.75$

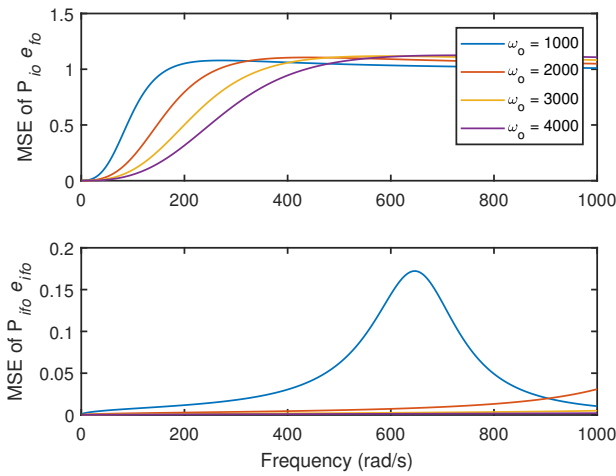


Fig. 4. The MSE curves with different ω_o when $a_o = 10$ and $\gamma = 0.75$

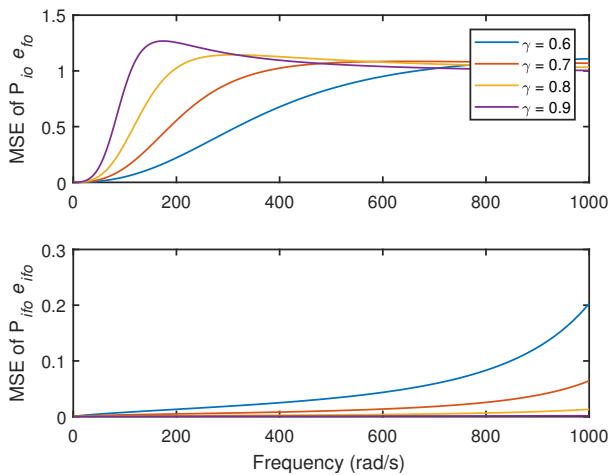


Fig. 5. The MSE curves with different γ when $a_o = 10$ and $\omega_o = 2000$

parameters.

V. TIME-DOMAIN SIMULATION AND COMPARISON

In this section, we will show the performance of the IFO-ADRC in the time-domain using MATLAB/Simulink and compare it with IO-ADRC and FO-ADRC. The plant used for the simulation is (24) which is adopted from the example of [1]. The structures of IFO-ADRC, FO-ADRC and IO-ADRC are similar and presented in Fig. 6, 7 and 8, respectively. An advantage of IFO-ADRC and FO-ADRC is that a simpler auxiliary controller u_0 can be used. Note that the auxiliary controller u_0 for IFO-ADRC and FO-ADRC is a P controller, while PD controllers must be used in IO-ADRC to ensure the stability. The controller in IFO-ADRC and FO-ADRC is

$$C_p(s) = K_{fp}, \quad (38)$$

where K_{fp} is the parameter of P controller and the PD controller in IO-ADRC is

$$C_{pd}(s) = K_{ip}(1 + K_{id}s), \quad (39)$$

where K_{ip} and K_{id} are the PD parameters. The IO-ESO used in IO-ADRC is given [17],

$$\begin{aligned} \dot{z} &= Az + Bu + L(y - \hat{y}) \\ \hat{y} &= Cz \end{aligned} \quad (40)$$

Refer to (25) for the matrices z , A , B , and C . The controller u in IO-ADRC is given

$$u = \frac{u_0 - \hat{f}_{io}}{b_0} \quad (41)$$

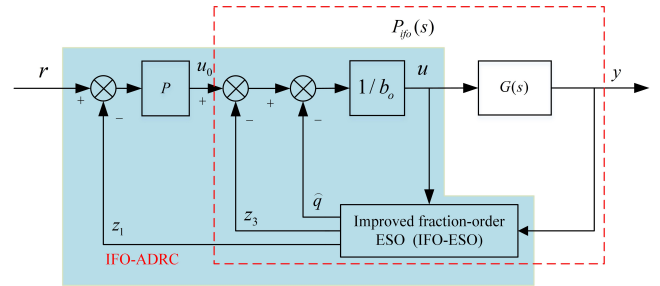


Fig. 6. Structure of the IFO-ADRC

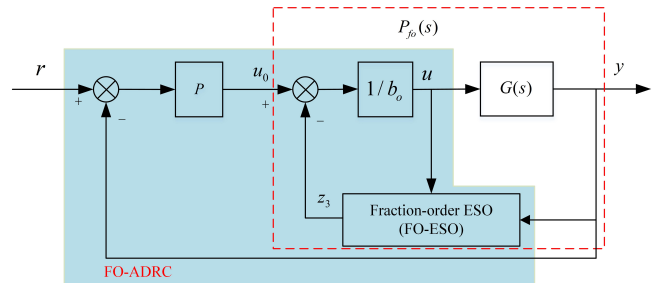


Fig. 7. Structure of the FO-ADRC in [1]

The observer gains $L = [\beta_1, \beta_2, \beta_3]^T = [3\omega_o, 3\omega_o^2, \omega_o^3]^T$ and the order γ are adopted from the reference paper [1], i.e., $a_o = 26.08$, $b_0 = 383.635$, $b = b_0$, $\omega_o = 700$ rad/s, and

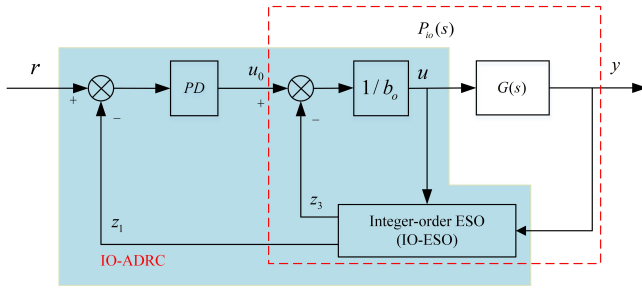


Fig. 8. Structure of the IO-ADRC

$\gamma = 0.75$. The fractional-order operator s^γ is discretized by the impulse response invariant method [27] where the discrete frequency for IFO-ESO and FO-ESO is 8000 Hz and the discrete order of the fractional-order operators is 7. Let the P controller parameter be $K_{fp} = 356$. Note that the observer parameters satisfy conditions of Theorem 3.2 and Theorem 1 in [1], the IFO-ADRC and FO-ADRC closed-loop systems are BIBO stable.

For the fair comparison, based on the open-loop transfer function, the PD controller used in IO-ADRC parameters are chosen to ensure that the gain crossover frequency ω_c^* and the phase margin φ_m of the IO-ADRC are the same as that of the IFO-ADRC [1], [11]. For IFO-ADRC, the open-loop transfer function can be described as

$$G_{iffo}(s) = C_p(s) \frac{Z_1(s)}{U_0(s)} = K_{fp} P_{iffo}(s) \frac{Z_1(s)}{Y(s)} \quad (42)$$

where

$$\frac{Z_1(s)}{Y(s)} = \frac{s^{2+\gamma} + 3\omega_o s^2 + a_o s^{1+\gamma} + 3\omega_o^2 s^\gamma + \omega_o^3}{s^{2+\gamma} + 3\omega_o s^2 + 3\omega_o^2 s^\gamma + \omega_o^3} \quad (43)$$

The gain crossover frequency $\omega_c^* = 42$ rad/s and the phase margin $\varphi_m = 39.9^\circ$ can be calculated from

$$\begin{aligned} \angle |G_{iffo}(j\omega_c^*)| &= -\pi + \varphi_m \\ |G_{iffo}(j\omega_c^*)| &= 1 \end{aligned} \quad (44)$$

For IO-ADRC, the open-loop transfer function is

$$G_{io}(s) = C_{pd}(s) P_{io}(s) \frac{Z_1(s)}{Y(s)} \quad (45)$$

where

$$\begin{aligned} P_{io}(s) &= \frac{Y(s)}{U_0(s)} = \frac{(s + \omega_o)^3}{s(a_o + s)(s + \omega_o)^3 - a_o \omega_o^3 s} \\ \frac{Z_1(s)}{Y(s)} &= \frac{s^3 + (3\omega_o + a_o)s^2 + 3\omega_o^2 s + \omega_o^3}{s^3 + 3\omega_o s^2 + 3\omega_o^2 s + \omega_o^3} \end{aligned} \quad (46)$$

Then, the PD controller for IO-ADRC can be designed as

$$C_{pd}(s) = 1559.83(1 + 0.0199s) \quad (47)$$

to ensure that the gain crossover frequency $\omega_c^* = 42$ rad/s and the phase margin $\varphi_m = 39.9^\circ$

The open-loop Bode diagram of the IO-ADRC and IFO-ADRC systems is illustrated in Fig. 9 showing that the two systems have the same gain crossover frequency $\omega_c^* = 42$ rad/s and phase margin $\varphi_m = 39.9^\circ$. From the open-loop Bode

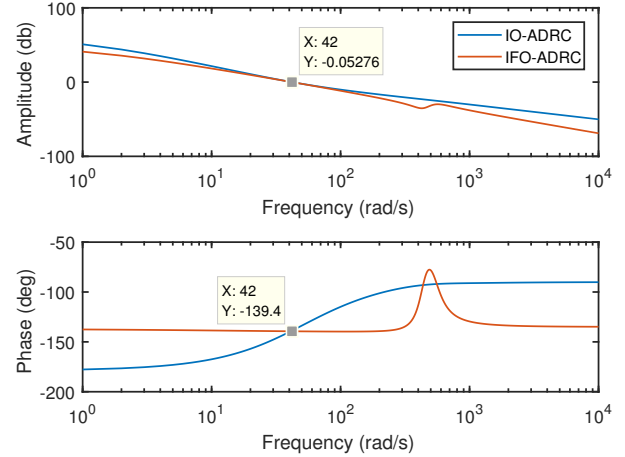


Fig. 9. Open-loop Bode diagram of the IO-ADRC system and the IFO-ADRC system

TABLE I
COMPARISON OF THE RESPONSES WITH THREE CONTROL SYSTEMS
(SIMULATION)

Controller	Overshoot(%) (K=1.0)	Settling time(s) (K=1.0)	Overshoot fluctuation(%) (K=0.8,1.0,1.2)
IO-ADRC	30.59	0.1928	5.601
FO-ADRC	61.03	0.3237	13.151
IFO-ADRC	30.66	0.1829	3.418

diagram of the IO-ADRC system, the IO-ADRC closed-loop system is stable.

The step responses of the IO-ADRC, FO-ADRC, and IFO-ADRC systems are shown in Fig. 10. It is shown in Fig. 10 that the IFO-ADRC system has better dynamic response performance than the FO-ADRC and IO-ADRC systems. The IFO-ADRC system has smaller overshoot than the FO-ADRC system.

Now, let us consider the system performance variation against controller parameters. Let us multiple the P controller parameter K_{fp} and PD controller parameter K_{ip} by $K = 0.8$ and $K = 1.2$. The nominal value is used when $K = 1$. Fig. 11, Fig. 12 and Fig. 13 are the step responses of three closed-loop systems when different controller parameters are imposed. As shown in Fig. 12 and Fig. 13, the IFO-ADRC system are robust to controller gain variations.

When $K = 0.8$, $K = 1.0$, or $K = 1.2$ are set respectively, the maximum speed of the step response are denoted as M_K . The overshoot fluctuation is calculated as

$$\text{overshoot fluctuation} = \frac{\max\{M_{0.8}, M_{1.0}, M_{1.2}\} - \min\{M_{0.8}, M_{1.0}, M_{1.2}\}}{\text{reference input}} \quad (48)$$

The step responses of three closed-loop systems for different K are given in TABLE I. Note that the overshoots of IFO-ADRC system and the IO-ADRC system are similar and smaller than that of the FO-ADRC system. The settling time

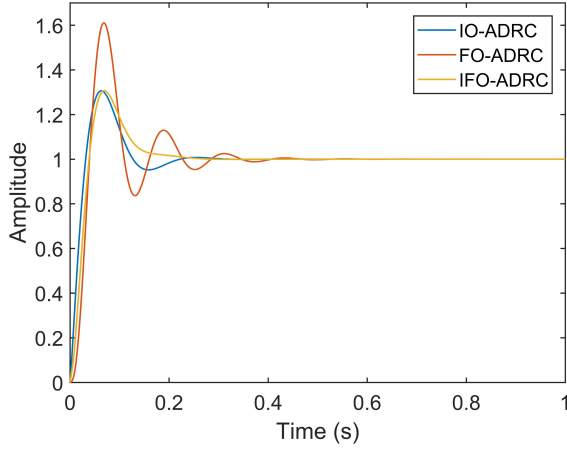


Fig. 10. Step responses of three different control systems

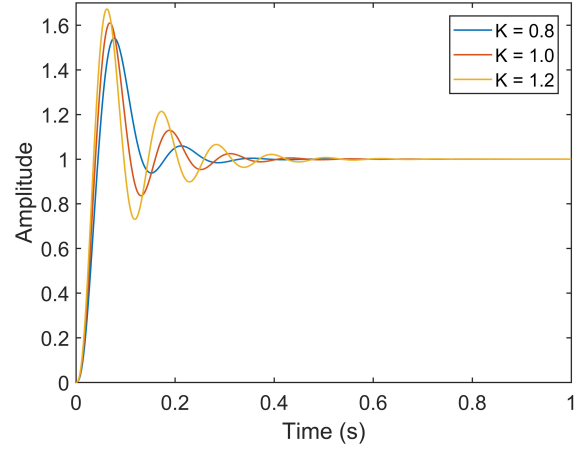


Fig. 12. Step responses of the FO-ADRC control system with controller gain variations

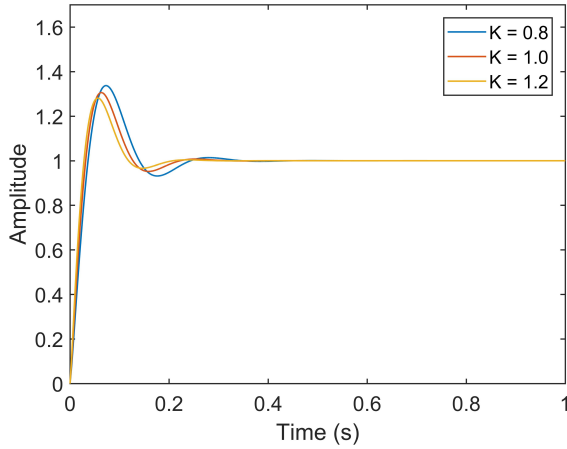


Fig. 11. Step responses of the IO-ADRC control system with controller gain variations

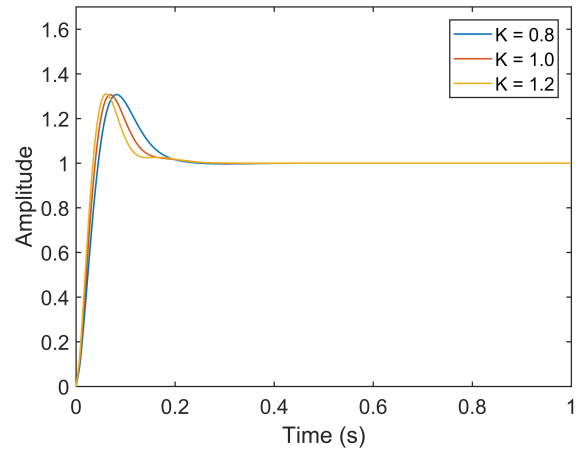


Fig. 13. Step responses of the IFO-ADRC control system with controller gain variations

of the IFO-ADRC system is shorter than the IO-ADRC and FO-ADRC systems.

VI. EXPERIMENTS: PMSM SPEED SERVO CONTROL

In this section, the control performance of IFO-ADRC, FO-ADRC, and IO-ADRC are compared in a real-world application. Experiments are carried out on the PMSM speed servo control system. Fig. 14 is the block diagram of the PMSM given in dq -axis frame. The diagram encircled by the blue and red dotted lines are the electromagnetic and the mechanical part of the PMSM, respectively.

The armature current of DC motor can be represented by q -axis component of the current i_q [8]. The q -axis voltage equation of PMSM is described as follows

$$u_q - E = u_q - C_e n = R_s i_q + L_q \frac{di_q}{dt} \quad (49)$$

where u_q is the q -axis voltage, E is the back electromotive force, C_e is the electromotive force coefficient, n is the actual speed of motor rotor, R_s is motor phase armature resistance, i_q is q -axis current and L_q is q -axis inductance. Taking u_q

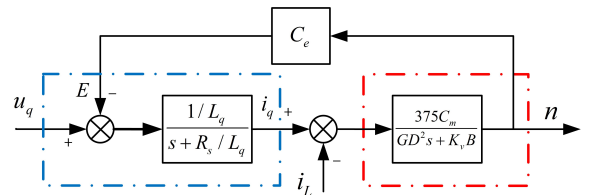


Fig. 14. Mathematical model of the PMSM

as the input voltage and i_q as the output current, the transfer functions of the electromagnetic part is

$$G_e(s) = \frac{I_q(s)}{U_q(s)} = \frac{1/L_q}{s + R_s/L_q} \quad (50)$$

where $I_q(s)$ and $U_q(s)$ are the Laplace transforms of i_q and u_q , respectively. Note that E is regarded as a constant disturbance input of the q -axis current loop and is therefore not shown in the transfer function above [28].

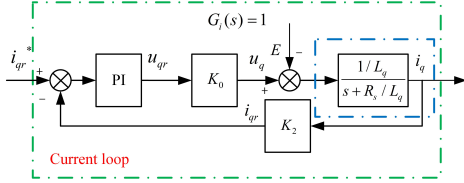
The motion equation of PMSM can be described as follows

$$T - T_L = C_m(i_q - i_L) = \frac{GD^2}{375} \frac{dn}{dt} + K_v B n \quad (51)$$

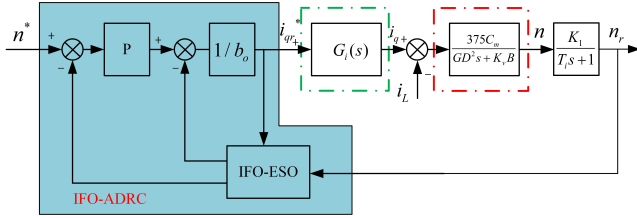
where T is the electromagnetic moment, T_L is the load moment, C_m is the torque coefficient, i_L is the equivalent current of load torque, GD^2 is flywheel inertia, K_v is a speed conversion factor, B is coefficient of viscous friction, and n is the actual speed of the motor rotor. Taking i_q as input current and n as output speed, the transfer functions of the mechanical part is

$$G_m = \frac{N(s)}{I_q(s)} = \frac{375C_m}{GD^2s + K_vB} \quad (52)$$

where $N(s)$ is the Laplace transforms of n . Note that the load moment is not considered in this paper, i.e., $i_L = 0$,



(a) Current loop of the PMSM speed servo system



(b) Speed loop of the PMSM speed servo system

Fig. 15. PMSM speed servo system using IFO-ADRC

The block encircled by the green dash-dotted line in Fig. 15(a) is the block diagram of the current loop $G_i(s)$ of the PMSM speed servo system. In Fig. 15(a), u_{qr} and i_{qr} are the per unit of the actual voltage and the actual current, respectively, i_{qr}^* is the reference input of the current loop, K_0 and K_2 are the voltage and current conversion factors, respectively. The PI controller in current loop is designed to ensure that $G_i(s) = 1$ in the operating frequency band of the speed loop. Fig. 15(b) is the block diagram of the speed loop of the PMSM speed servo system using IFO-ADRC. In Fig. 15(b), K_1 is the speed conversion factor, T_i is the speed feedback filter coefficient, and n_r is the per unit of the actual speed. Since $G_i(s) = 1$, thus the plant of the speed loop is

$$G(s) = \frac{N_r(s)}{I_q(s)} = \frac{375C_mK_1}{T_iGD^2s^2 + (K_vBT_i + GD^2)s + K_vB} \quad (53)$$

where $N_r(s)$ and $I_q(s)$ are Laplace transforms of n_r and i_q , respectively.

The closed-loop controller is implemented on digital signal processor (DSP) illustrated in Fig. 16. The PMSM is 60ST-M00630C and MOSFET is adopted as the gate driver. The specification of the PMSM is shown in TABLE II. $K_0 = 20.3$ is determined by the actual hardware, $K_1 = 1/1200$, $K_2 = 1/9.9$, $T_i = 1/100$ are configured by software, and $K_v = 30/\pi$ is the speed conversion factor from rad/s to r/min. The speed sampling period was set as 0.125 ms, and the current loop sampling period is set as 0.0625 ms. The motor speed waveform is collected by DSP Emulator and CCS software.

TABLE II
THE SPECIFICATION OF THE PMSM

Parameters	Unit	Value
R_s	Ω	0.3
L_q	mH	1.377
GD^2	Kgm ²	0.00147
B	Ns/rad	0.05880
C_m	Nm/A	0.112

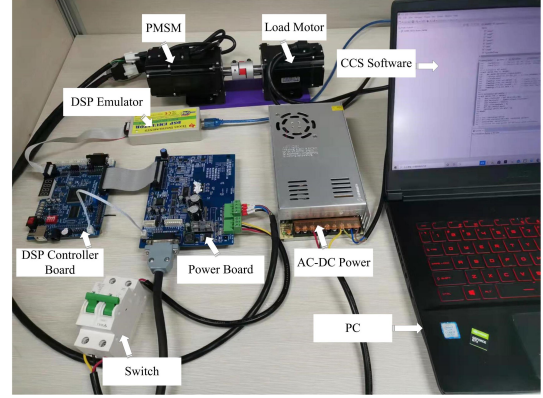


Fig. 16. Experimental platform for control performance validation

When the specification of the PMSM in Table II is used, the plant (53) of the PMSM becomes

$$G(s) = \frac{2380.9}{s^2 + 138.1s + 3819.7} \quad (54)$$

We use the same controllers in Section V for IFO-ADRC, FO-ADRC and IO-ADRC. Let the observer gain be $L = [\beta_1, \beta_2, \beta_3]^T = [3\omega_0, 3\omega_0^2, \omega_0^3]^T$, $\omega_0 = 700$ rad/s, and $\gamma = 0.75$. The operator s^γ is discretized by the impulse response invariant method where the discrete frequency is 8000 Hz and the discrete order of the fractional-order operators is 5. The parameter of the P controller (see (38)) used in the IFO-ADRC and the FO-ADRC is $K_{fp} = 750$, while the PD controller used in the IO-ADRC design method in Section V is designed as

$$C_{pd}(s) = 2314.69(1 + 0.0185s) \quad (55)$$

For the IFO-ADRC closed-loop system, all parameters meet the conditions of Theorem 3.2, thus the closed-loop of IFO-ADRC is BIBO stable. Also, the IO-ADRC and FO-ADRC closed-loop systems are ensured to be BIBO stable.

Let us multiple the P controller parameter K_{fp} and PD controller parameter K_{ip} by $K = 0.6$ and $K = 1.4$, while the nominal value is used when $K = 1$. Fig. 18 and Fig. 19 are simulation results of step responses with different controller parameters for the FO-ADRC and IFO-ADRC systems, respectively. As shown in Fig. 18 and Fig. 19, the IFO-ADRC system is robust to the controller parameter variations. Fig. 20 is step responses of the IO-ADRC, FO-ADRC and IFO-ADRC systems for the experiment setup. It is illustrated that the step response of the IFO-ADRC system has smaller overshoot, oscillation magnitude and shorter settling time than the FO-ADRC and IO-ADRC system. Fig. 22 and Fig. 23 are experiment results of step responses of three

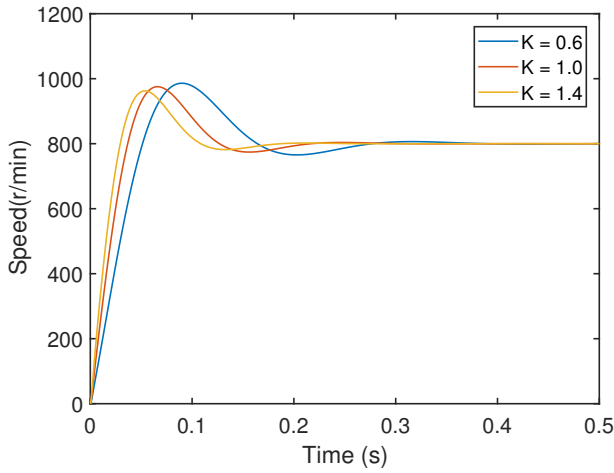


Fig. 17. Step responses of the IO-ADRC control system with controller gain variations (simulation)

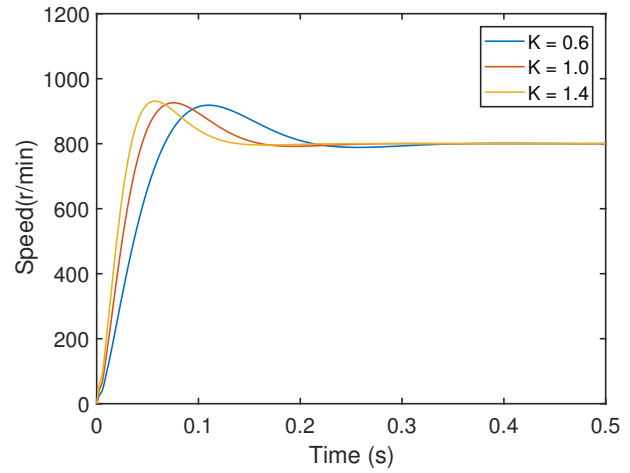


Fig. 19. Step responses of the IFO-ADRC control system with controller gain variations (simulation)

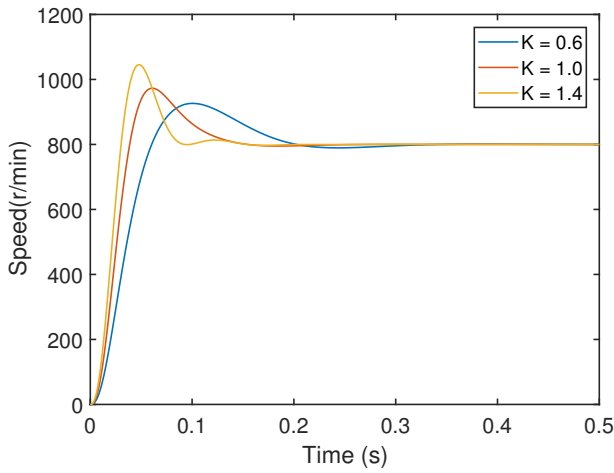


Fig. 18. Step responses of the FO-ADRC control system with controller gain variations (simulation)

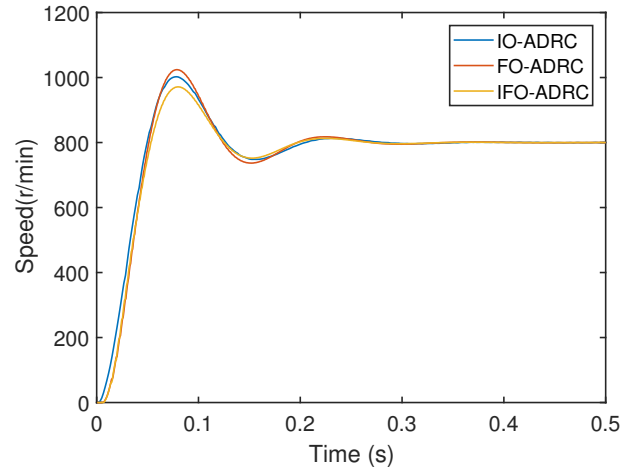


Fig. 20. Step responses of three different control methods (experiment)

different systems when the controller parameter varies. Similar to simulation result, the IFO-ADRC system is the most robust to controller parameter variations. Table III summarizes results of the step responses for three different systems, showing that the IFO-ADRC system has smaller overshoot, less settling time, and overshoot fluctuation than the IO-ADRC and FO-ADRC system.

TABLE III
COMPARISON OF THE RESPONSES WITH THREE CONTROL SYSTEMS
(EXPERIMENT)

Controller	Overshoot(%) (K=1.0)	Settling time(s) (K=1.0)	Overshoot fluctuation(%) (K=0.6,1.0,1.4)
IO-ADRC	25.30	0.191	4.883
FO-ADRC	28.03	0.233	15.035
IFO-ADRC	21.40	0.185	2.584

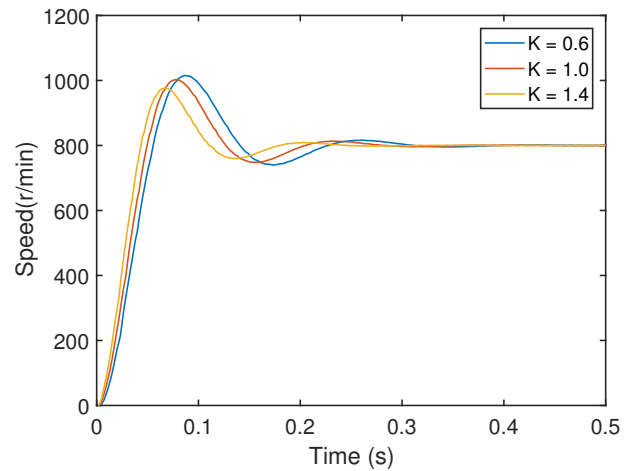


Fig. 21. Step responses of the IO-ADRC with controller gain variations (experiment)

VII. CONCLUSION

An improved active disturbance rejection control scheme with IFO-ESO is proposed in this paper. IFO-ESO can ap-

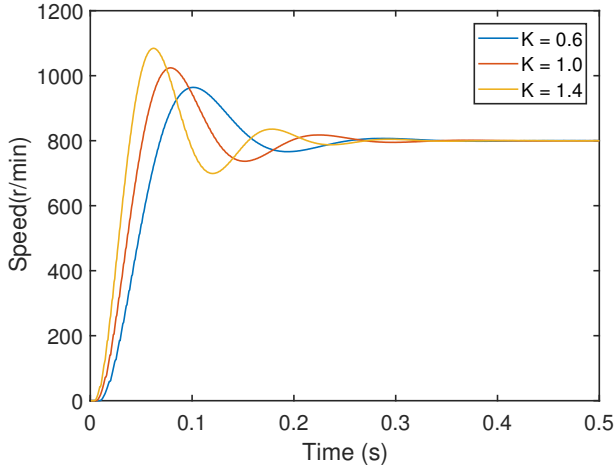


Fig. 22. Step responses of the FO-ADRC with controller gain variations (experiment)

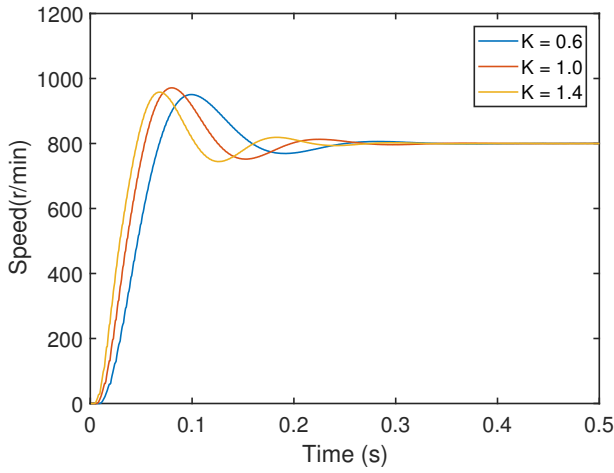


Fig. 23. Step responses of the IFO-ADRC with controller gain variations (experiment)

proximately convert an integer-order system into a cascaded fractional-order integrator for which a simpler feedback law can be designed. The approximation to a cascaded fractional-order integrator by IFO-ESO behaves well across a larger frequency band than FO-ESO, ensuring the closed-loop system is robust to controller gain, ESO parameters, and plant parameters variations. The frequency-domain analysis and PMSM speed servo control experiments verify that the proposed IFO-ADRC achieves better performance than FO-ADRC and IO-ADRC.

APPENDIX

Proof of Theorem 3.1: Let $w = s^{\nu+\gamma}$, and (17) can be written:

$$\lambda(w) = w(w^{n\sigma} + \sum_{i=1}^{n-1} \beta_i w^{(n-i)\sigma}) + \beta_n w^\sigma + \beta_{n+1} \quad (56)$$

where $\sigma = \frac{\gamma}{\nu+\gamma}$, $0 < \sigma < 1$. According to Kharitonov-Based Method [29], the two boundary polynomials are:

$$\begin{aligned} {}^1\lambda(w) &= w(1 + \sum_{i=1}^{n-1} \beta_i) + \beta_n + \beta_{n+1} \\ {}^2\lambda(w) &= w(w^n + \sum_{i=1}^{n-1} \beta_i w^{(n-i)}) + \beta_n w + \beta_{n+1} \end{aligned} \quad (57)$$

Substitute $\beta_i = C_{n+1}^i \omega_o^i$, $i = 1, 2, \dots, n+1$ into ${}^2\lambda(w)$ gives ${}^2\lambda(w) = (w + \omega_o)^{n+1}$. Then, the roots of the two boundary polynomials are:

$$\begin{aligned} {}^1\lambda(w) : w_1 &= -\frac{n\omega_o^n + \omega_o^{n+1}}{(1 + \sum_{i=1}^{n-1} C_{n+1}^i \omega_o^i)} \\ {}^2\lambda(w) : w_i &= -\omega_o, i = 1, 2, 3 \dots, n+1 \end{aligned} \quad (58)$$

Since all the roots of the boundary polynomials are located in $|\arg(w_i)| > \frac{\pi}{2(\nu+\gamma)}$, all the roots of (56) are located in $|\arg(w_i)| > \frac{\pi}{2(\nu+\gamma)}$ [30], i.e., $\lambda(s)$ is Hurwitz, system (15) is BIBO stable, regarding h_{ifo} as input and e_1 as output. ■

Proof of Theorem 3.2:

Let $(r_1, r_2, r_3 \dots r_m, r_{m+1}) = (r, r^{(1)}, r^{(2)}, \dots, r^{(m-1)}, r^{(n\gamma-m+1)})$. From (6) and (15), one has

$$\begin{aligned} y^{(n\gamma)} &= k_p(r_1 - z_1) + k_{d1}(\dot{r}_1 - \dot{z}_1) + \dots + k_{d_{m-2}}(r_1^{(m-2)} \\ &\quad - z_1^{(m-2)}) + r_1^{(n\gamma)} + f_{ifo} - \hat{f}_{ifo} + q - \hat{q} \end{aligned} \quad (59)$$

It follows from (14) that

$$\begin{aligned} y^{(n\gamma)} - r_1^{(n\gamma)} &= k_p(r_1 - x_1 + e_1) + k_{d1}(\dot{r}_1 - \dot{x}_1 + \dot{e}_1) + \dots \\ &\quad + k_{d_{m-2}}(r_1^{(m-2)} - x_1^{(m-2)} + e_1^{(m-2)}) \\ &\quad + e_{n+1} + e_n^{(\gamma)} - e_n^{(x)} \end{aligned} \quad (60)$$

Let $q_1 = r_1 - x_1$, $q_i = \dot{q}_{i-1}$, $i = 2, 3, \dots, v-1$, (60) can be written as

$$\begin{aligned} \dot{q}_1 &= q_2, \dot{q}_2 = q_3, \dots, \dot{q}_{m-1} = q_m \\ q_m^{(n\gamma-m+1)} &= q_{m+1} = -(k_p q_1 + k_{d1} q_2 + \dots + k_{d_{m-2}} q_{m-1}) \\ &\quad - (k_p e_1 + k_{d1} \dot{e}_1 + \dots + k_{d_{m-2}} e_1^{(m-2)}) \\ &\quad - e_{n+1} - e_n^{(\gamma)} + e_n^{(x)} \end{aligned} \quad (61)$$

The system (15) can be written:

$$\begin{aligned} e_1^{(\gamma)} &= -\beta_1 e_1 + e_2 \\ e_2^{(\gamma)} &= -\beta_2 e_1 + e_3 \\ &\vdots \\ \frac{d^{(x)} e_n}{d^{(x)} t} &= -\beta_n e_1 + e_{n+1} \\ e_{n+1}^{(\gamma)} &= -\beta_{n+1} e_1 + h_{ifo} \\ h_{ifo} &= a_0 q_1^{(\gamma)} + a_1 q_2^{(\gamma)} + a_2 q_3^{(\gamma)} \\ &\quad + \dots + a_{m-1} q_m^{(\gamma)} + R \end{aligned}$$

where

$$R = -\sum_{i=1}^{n-1} a_i r_{i+1}^{(\gamma)} - a_0 r_1^{(\gamma)} + d \quad (62)$$

According to (61), it follows that,

$$\begin{aligned} q_m^{(n\gamma-m+1)} &= q_{m+1} = -(k_p q_1 + k_{d_1} q_2 + \cdots + k_{d_{m-2}} q_{m-1}) \\ &\quad - (k_p e_1 + k_{d_1} \dot{e}_1 + \cdots + k_{d_{m-2}} e_1^{(m-2)}) \\ &\quad - e_n^{(\gamma)} - \beta_n e_1 \end{aligned} \quad (63)$$

Note $w_1 = k_p e_1 + k_{d_1} \dot{e}_1 + \cdots + k_{d_{m-2}} e_1^{(m-2)} + e_n^{(\gamma)} + \beta_n e_1$, $w_2 = a_0 q_1^{(\gamma)} + a_1 q_2^{(\gamma)} + a_2 q_3^{(\gamma)} + \cdots + a_{m-1} q_m^{(\gamma)}$. Combining (63) and (62) gives the block diagram of the closed-loop system in Fig. 24. From (63), it gives

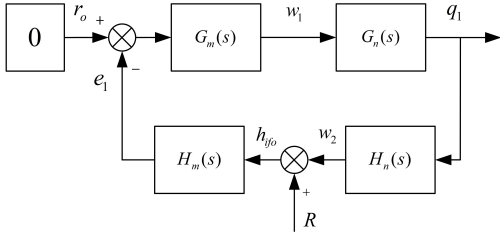


Fig. 24. The block diagram of the closed-loop system

$$\begin{aligned} G_m(s) &= -\frac{W_1(s)}{E(s)} = k_p + \sum_{i=1}^{m-2} k_{d_i} s^i + s^{n\gamma} + \sum_{i=1}^n \beta_i s^{(n-i)\gamma} \\ G_n(s) &= \frac{Q_1(s)}{W_1(s)} = \frac{1}{s^{n\gamma} + k_p + \sum_{i=1}^{m-2} k_{d_i} s^i} \end{aligned} \quad (64)$$

where $W_1(s)$, $Q_1(s)$ and $E_1(s)$ are the Laplace transforms of signals w_1 , q_1 and e_1 , respectively. According to (62), one has

$$\begin{aligned} H_m(s) &= \frac{E_1(s)}{H_f(s)} = \frac{1}{s^{\nu+\gamma}(s^{n\gamma} + \sum_{i=1}^{n-1} \beta_i s^{(n-i)\gamma}) + \beta_n s^\gamma + \beta_{n+1}} \\ H_n(s) &= \frac{W_2(s)}{Q_1(s)} = s^\gamma \sum_{i=0}^{m-1} a_i s^i \end{aligned} \quad (65)$$

where $H_f(s)$ and $W_2(s)$ are the Laplace transforms of signals h_{fo} and w_2 , respectively.

Now, let us show R is bounded. Let $d_0 = \sum_{i=0}^{m-2} C_m^i v^{m-i} r_{i+1} + r_{m+1}$ where $v > 0$ and

$d_1 = \sum_{i=1}^{n-1} a_i r_{i+1}^{(\gamma)} + a_0 r_1^{(\gamma)}$. Define the transfer function of the system as

$$P_1(s) = \frac{D_1(s)}{D_0(s)} = \frac{\sum_{i=1}^{n-1} a_i s^{(i+\gamma)} + a_0 s^{(\gamma)}}{s^{n\gamma} + \sum_{i=0}^{m-2} C_m^i v^{m-i} s^i} \quad (66)$$

where $D_0(s)$ and $D_1(s)$ are the Laplace transforms of d_0 and d_1 , respectively. Similar to the proof of (17), the characteristic polynomial of the system $P_1(s)$ is Hurwitz, i.e., the system $P_1(s)$ is BIBO stable. As a result, $r_1, r_2, r_3 \cdots r_m, r_{m+1}$ are bounded, i.e., d_0 is bounded, then d_1 is bounded. Note that $R = -d_1 + d$. Since d is bounded, R is bounded.

Because R is bounded, we can treat R as the disturbance and calculate the transfer function of the closed-loop system. Further calculation gives

$$G_o(s) = -\frac{Q_1(s)}{E(s)} = G_m(s)G_n(s) \quad (67)$$

$$H_o(s) = \frac{E_1(s)}{Q_1(s)} = H_m(s)H_n(s) \quad (68)$$

Combining (67) and (68), the transfer function of the closed-loop system $P_o(s)$ can be given

$$P_o(s) = \frac{Q_1(s)}{R_o(s)} = \frac{G_o(s)}{1 + G_o(s)H_o(s)} \quad (69)$$

where $R_o(s)$ is the Laplace transforms of r_o (see the Fig. 24). The characteristic polynomial of the closed-loop system is

$$\begin{aligned} P(s) &= (s^\gamma \sum_{i=0}^{m-1} a_i s^i)(k_p + \sum_{i=1}^{m-2} k_{d_i} s^i + s^{n\gamma} + \sum_{i=1}^n \beta_i s^{(n-i)\gamma}) \\ &\quad + (s^{n\gamma} + k_p + \sum_{i=1}^{m-2} k_{d_i} s^i)(s^{\nu+\gamma}(s^{n\gamma} + \sum_{i=1}^{n-1} \beta_i s^{(n-i)\gamma}) \\ &\quad + \beta_n s^\gamma + \beta_{n+1}) \end{aligned} \quad (70)$$

Finding prime number p_1, p_2, q_1 , and q_3 such that $\nu = \frac{p_1}{q_1}$, $\gamma = \frac{p_2}{q_2}$, (18) is satisfied. Since R is bounded, the closed-loop system is BIBO stable [29]. ■

Proof of Proposition 3.2: When $m = n = 2$, the characteristic polynomial $P(s)$ of the closed-loop system can be written

$$P(s) = s^\gamma (a_0 + a_1 s)(k_p + s^{2\gamma} + \beta_1 s^\gamma + \beta_2) \quad (71)$$

$$+ (s^{2\gamma} + k_p)(s^{2+\gamma} + \beta_1 s^2 + \beta_2 s^\gamma + \beta_3) \quad (72)$$

According to Kharitonov-Based Method, when $\beta_i = C_{n+1}^i \omega_o^i$ for $i = 1, 2, 3$, the two boundary polynomial can be written

$${}^1P(s) = A_0 s^2 + A_1 s + A_2$$

$${}^2P(s) = B_0 s^5 + B_1 s^4 + B_2 s^3 + B_3 s^2 + B_4 s + B_5 \quad (73)$$

where

$$A_0 = 1 + k_p + 3(1 + k_p)\omega_o$$

$$A_1 = a_1(1 + k_p + 3\omega_o + 3\omega_o^2)$$

$$A_2 = a_0(1 + k_p + 3\omega_o + 3\omega_o^2) + 3(1 + k_p)\omega_o^2 + (1 + k_p)\omega_o^3$$

$$B_0 = 1, B_1 = a_1 + 3\omega_o, B_2 = a_0 + k_p + 3a_1\omega_o + 3\omega_o^2$$

$$B_3 = a_1 k_p + 3a_0\omega_o + 3k_p\omega_o + 3a_1\omega_o^2 + \omega_o^3$$

$$B_4 = a_0 k_p + 3a_0\omega_o^2 + 3k_p\omega_o^2, B_5 = k_p\omega_o^3 \quad (74)$$

Firstly, we consider ${}^1P(s) = 0$. When $a_1 \geq 0$, $a_0 \geq 0$, $k_p > 0$, and $\omega_o > 0$, from (74), we have $A_0 > 0$, $A_1 \geq 0$, and $A_2 > 0$. According to Routh-Hurwitz criterion, if $a_1 \geq 0$, $a_0 \geq 0$, $k_p > 0$, and $\omega_o > 0$, all the roots of ${}^1P(s) = 0$ are located in left plane, i.e., when $a_1 \geq 0$ and $a_0 \geq 0$, there exists a sufficiently large $\omega_o > 0$, such that all the root of ${}^1P(s) = 0$ are located in left plane.

Secondly, we consider ${}^2P(s) = 0$. According to Routh-Hurwitz criterion, ${}^2P(s) = 0$ can be written as the Routh

TABLE IV
ROUTH TABLE OF ${}^2P(s) = 0$

s^5	B_0	B_2	B_4
s^4	B_1	B_3	B_5
s^3	C_1	C_5	
s^2	C_2	C_6	
s^1	C_3		
s^0	C_4		

table form

In TABLE IV, $C_1, C_2, C_3,$ and C_4 are

$$C_1 = \frac{N_5}{D_5}, C_2 = \frac{N_6}{D_6}, C_3 = \frac{N_7}{D_7}, C_4 = k_p \omega_o^3 \quad (75)$$

where

$$N_5 = a_0 a_1 + 3a_1^2 \omega_o + 9a_1 \omega_o^2 + 8\omega_o^3$$

$$D_5 = a_1 + 3\omega_o$$

$$N_6 = 3a_1(a_0^2 + a_1^2 k_p) \omega_o + (9a_0 a_1^2 + 15a_1^2 k_p) \omega_o^2 + a_1(10a_0 + 9a_1^2 + 18k_p) \omega_o^3 + 30a_1^2 \omega_o^4 + 33a_1 \omega_o^5 + 8\omega_o^6 - 3a_1 a_0 k_p - 9a_0 k_p - 3a_0 \omega_o^4$$

$$D_6 = a_0 a_1 + 3a_1^2 \omega_o + 9a_1 \omega_o^2 + 8\omega_o^3$$

$$N_7 = 3(a_0^3 a_1 k_p + a_0 a_1^3 k_p^2) + (9a_0^2 a_1^2 k_p + 15a_0 a_1^2 k_p^2) \omega_o + (9a_0^3 a_1 + 9a_0^2 a_1 k_p + 18a_0 a_1^3 k_p + 9a_0 a_1 k_p^2 + 9a_1^3 k_p^2) \omega_o^2 + (27a_0^2 a_1^2 + 96a_0 a_1^2 k_p - 24a_0 k_p^2 + 42a_1^2 k_p^2) \omega_o^3 + (30a_0^2 a_1 + 27a_0 a_1^3 + 108a_0 a_1 k_p + 18a_1^3 k_p + 48a_1 k_p^2) \omega_o^4 + (90a_0 a_1^2 + 54a_1^2 k_p) \omega_o^5 + (99a_0 a_1 + 48a_1 k_p) \omega_o^6 + 24a_0 \omega_o^7 - 3a_0^2 a_1 k_p^2 - 9a_0^2 k_p^2 \omega_o - 30a_0^2 k_p \omega_o^3 - 9a_0^2 \omega_o^5$$

$$D_7 = 3a_1(a_0^2 + a_1^2 k_p) + (9a_0 a_1^2 + 15a_1^2 k_p) \omega_o + a_1(10a_0 + 9a_1^2 + 18k_p) \omega_o^2 + 30a_1^2 \omega_o^3 + 33a_1 \omega_o^4 + 8\omega_o^5 - 3a_1 a_0 k_p - 9a_0 k_p \omega_o - 3a_0 \omega_o^3 \quad (76)$$

When $a_0 \geq 0, a_1 \geq 0,$ and ω_o is sufficiently large, from (76), we have $B_0 > 0, B_1 > 0, C_1 > 0, C_2 > 0, C_3 \geq 0,$ and $C_4 > 0.$ According to Routh-Hurwitz criterion, if $B_0 > 0, B_1 > 0, C_1 > 0, C_2 > 0, C_3 \geq 0,$ and $C_4 > 0,$ then all the roots of ${}^2P(s) = 0$ are located in the left plane.

In summary, choosing $\beta_i = C_{n+1}^i \omega_o^i$ for $i = 1, 2, 3,$ when $m = n = 2, a_1 \geq 0$ and $a_0 \geq 0,$ there always exists a constant $\omega_o > 0,$ such that the closed-loop is BIBO stable. ■

REFERENCES

- [1] P. Chen, Y. Luo, W. Zheng, Z. Gao, and Y. Chen, "Fractional order active disturbance rejection control with the idea of cascaded fractional order integrator equivalence," *ISA transactions*, vol. 114, pp. 359–369, 2021.
- [2] L. Liu, H. Xing, X. Cao, Z. Fu, and S. Song, "Guaranteed cost finite-time control of discrete-time positive impulsive switched systems," *Complexity*, vol. 2018, 2018.
- [3] Y.-F. Pu, Z. Yi, and J.-L. Zhou, "Fractional hopfield neural networks: Fractional dynamic associative recurrent neural networks," *IEEE transactions on neural networks and learning systems*, vol. 28, no. 10, pp. 2319–2333, 2016.
- [4] G. Tzounas, I. Dassios, M. A. A. Murad, and F. Milano, "Theory and implementation of fractional order controllers for power system applications," *IEEE Transactions on Power Systems*, vol. 35, no. 6, pp. 4622–4631, 2020.
- [5] Y. Luo and Y. Chen, "Fractional order [proportional derivative] controller for a class of fractional order systems," *Automatica*, vol. 45, no. 10, pp. 2446–2450, 2009.
- [6] S. K. Mishra and D. Chandra, "Fractional order modeling of continuous highorder mimo systems," in *2013 IEEE International Conference on Signal Processing, Computing and Control (ISPC)*. IEEE, 2013, pp. 1–5.
- [7] Y. Chen, I. Petras, and D. Xue, "Fractional order control-a tutorial," in *2009 American control conference*. IEEE, 2009, pp. 1397–1411.
- [8] W. Zheng, Y. Luo, Y. Chen, and Y. Pi, "Fractional-order modeling of permanent magnet synchronous motor speed servo system," *Journal of Vibration and Control*, vol. 22, no. 9, pp. 2255–2280, 2016.
- [9] P. Nataraj and R. Kalla, "Computation of spectral sets for uncertain linear fractional-order systems," *Communications in Nonlinear Science and Numerical Simulation*, vol. 15, no. 4, pp. 946–955, 2010.
- [10] I. Podlubny, L. Dorcak, and I. Kostial, "On fractional derivatives, fractional-order dynamic systems and pi/sup/spl lambda/d/sup/spl mu/-controllers," in *Proceedings of the 36th IEEE Conference on Decision and Control*, vol. 5. IEEE, 1997, pp. 4985–4990.
- [11] W. Zheng, Y. Luo, Y. Chen, and X. Wang, "Synthesis of fractional order robust controller based on bode's ideas," *ISA transactions*, vol. 111, pp. 290–301, 2021.
- [12] F. M. Zaihidee, S. Mekhilef, and M. Mubin, "Application of fractional order sliding mode control for speed control of permanent magnet synchronous motor," *IEEE Access*, vol. 7, pp. 101 765–101 774, 2019.
- [13] H.-P. Ren, X. Wang, J.-T. Fan, and O. Kaynak, "Fractional order sliding mode control of a pneumatic position servo system," *Journal of the Franklin Institute*, vol. 356, no. 12, pp. 6160–6174, 2019.
- [14] A. Gomaa Haroun and L. Yin-Ya, "A novel optimized fractional-order hybrid fuzzy intelligent PID controller for interconnected realistic power systems," *Transactions of the Institute of Measurement and Control*, vol. 41, no. 11, pp. 3065–3080, 2019.
- [15] H. Li, Y. Luo, and Y. Chen, "A fractional order proportional and derivative (FOPD) motion controller: tuning rule and experiments," *IEEE Transactions on control systems technology*, vol. 18, no. 2, pp. 516–520, 2009.
- [16] J. Q. Han, "From PID technique to active disturbances rejection control technique," *Basic Automation*, 2002.
- [17] Z. Gao, "Scaling and bandwidth-parameterization based controller tuning," in *Proceedings of the American control conference*, vol. 6, 2006, pp. 4989–4996.
- [18] —, "Active disturbance rejection control for nonlinear fractional-order systems," *International Journal of Robust and Nonlinear Control*, vol. 26, no. 4, pp. 876–892, 2016.
- [19] P. Kumar and S. K. Chaudhary, "Stability analysis and fractional order controller design for control system," *International Journal of Applied Engineering Research*, vol. 12, no. 20, pp. 10298–10304, 2017.
- [20] S. K. Choudhary, "Stability and performance analysis of fractional order control systems," *Wseas Transactions on Systems and Control*, vol. 9, no. 45, pp. 438–444, 2014.
- [21] R. Trivedi and P. K. Padhy, "Design of indirect fractional order imc controller for fractional order processes," *IEEE Transactions on Circuits and Systems II: Express Briefs*, vol. 68, no. 3, pp. 968–972, 2020.
- [22] D. Li, P. Ding, and Z. Gao, "Fractional active disturbance rejection control," *ISA transactions*, vol. 62, pp. 109–119, 2016.
- [23] M. Li, D. Li, J. Wang, and C. Zhao, "Active disturbance rejection control for fractional-order system," *ISA transactions*, vol. 52, no. 3, pp. 365–374, 2013.
- [24] C. Li, D. Qian, and Y. Chen, "On riemann-liouville and caputo derivatives," *Discrete Dynamics in Nature and Society*, vol. 2011, 2011.
- [25] W. Deng, C. Li, and J. Lü, "Stability analysis of linear fractional differential system with multiple time delays," *Nonlinear Dynamics*, vol. 48, no. 4, pp. 409–416, 2007.
- [26] M. H. Richardson and D. L. Formenti, "Parameter estimation from frequency response measurements using rational fraction polynomials," in *Proceedings of the 1st international modal analysis conference*, vol. 1. Union College Schenectady, NY, 1982, pp. 167–186.

- [27] Y. Chen, "Impulse response invariant discretization of fractional order integrators/differentiators," May 2009, uRL <http://www.mathworks.com/matlabcentral/leexchange/21342impulseresponse-invariant-discretization-of-fractional-orderintegrators-differentiator>.
- [28] Y. Ruan and B. Chen, "Control systems of electric drives-motion control systems," 2010.
- [29] I. Petráš, Fractional-order nonlinear systems: modeling, analysis and simulation. Springer Science & Business Media, 2011.
- [30] I. Petráš, Y. Chen, and B. M. Vinagre, "A robust stability test procedure for a class of uncertain lti fractional order systems," in Proc. of ICC2002, May, 2002, pp. 27–30.